3 Seismology and Earth Structure

Ordinary language undergoes modification to a high pressure form when applied to the interior of the earth; a few examples of equivalents follow:

Ordinary meaning:	*High pressure form:*
dubious	*certain*
perhaps	*undoubtedly*
vague suggestion	*positive proof*
trivial objection	*unanswerable argument*
uncertain mixture of all the elements	*pure iron*

Francis Birch, 1952

3.1 Introduction

A major application of seismology is the determination of the distribution of seismic velocities, and hence elastic properties, within the earth. This distribution, known as *earth structure*, gives the basic constraint on the mineralogical, chemical, and thermal state of the earth's interior. Seismological data are important for this purpose because their resolving power is generally superior to that of other geophysical methods. For example, although gravity and magnetic data indicate the presence of a dense fluid core at depth, they provide only relatively weak constraints on its density and size. By contrast, seismological data indicate the depth of the core–mantle boundary and the sharp change in properties that occurs there. Above the boundary, both *P* and *S* waves propagate in the solid mantle, whereas in the liquid outer core no *S* waves propagate and the *P*-wave velocity drops sharply. The observed velocities are the primary basis for our models of the physical properties and chemical composition of the material on either side of this boundary. Similarly, the distinction between the crust and the mantle and many inferences about their structure and composition come from seismological observations. More generally, by establishing the essentially layered structure of the earth, seismology provides the primary evidence for the process of differentiation whereby material within planets became compositionally segregated during their evolution. As a result, many crucial issues about the other terrestrial planets could be resolved if seismological data were available.

Constraints from seismology are crucial for other disciplines of the earth sciences, and vice versa. Seismology gives *earth models* describing the distribution of *P*- and *S*-wave velocities and density. Going from an earth model to a description of the chemical, mineralogical, thermal, and rheological state of the earth's interior requires additional information. There are thus two types of uncertainty in our knowledge of the earth's interior. In some cases, such as the structure of the inner core, the seismological results are still under discussion. In others — for example, the nature of the 660 km discontinuity in the mantle — the basic seismological results are generally accepted, but their mineralogic and petrologic interpretations remain under investigation. Given our scope here, we only summarize the implications of seismological data for models of the earth's interior.

The fundamental data for seismological studies of the earth's interior are the travel times of seismic waves. The measurements available are the arrival times of seismic waves at receivers. To convert these to travel times, the origin time and location of the source must be known. These parameters, which are known for artificial sources, must be estimated from the observations for earthquake sources. Hence travel time data include information about both the source and the properties of the medium, and separating the two is a challenge in many seismological studies.

The travel times are used to learn about the velocity structure between the source and the receiver. As we saw in the last chapter, waves follow paths that depend on the velocity

structure. Hence the structure must be known to find the paths that the waves took. To illustrate this, consider the travel time between two points. If the velocity were constant, the ray path would be a straight line, and the velocity could be found by dividing the distance by the travel time. If, instead, an interface separates media with different velocities, the ray path would consist of two line segments, depending on the velocities, and the travel time would be the sum of the time spent along each segment. For a more complicated velocity distribution, the ray path would also be more complicated.

This problem can be posed mathematically by writing the travel time between the source (s) and receiver (r) as the integral of 1/velocity, or slowness, along the ray path

$$T(s, r) = \int_s^r \frac{1}{v(x)}\, dx. \tag{1}$$

In simple cases, where the ray path is a set of segments with constant velocity, the integral is just a sum over the time in each segment. Thus the travel time gives an integral constraint on the velocity distribution between the source and the receiver, but does not indicate which of the many paths satisfying the constraint the ray followed. As a result, an individual measurement is inadequate to show the distribution of velocities. Fortunately, as we shall see, a set of travel times between different sources and receivers provides much more information. In addition, useful information is derived from the amplitudes and waveforms of seismic waves.

This example illustrates an interesting feature of determining velocity structure from travel times. If the velocity structure is known, the forward problem of finding the travel times and amplitudes is straightforward. However, the inverse problem of using the travel times and amplitudes measured at the surface to find the velocity structure at depth is more difficult, and various methods are used. For example, in addition to using travel times directly, we have seen that velocity structure is studied using the dispersion of surface waves (Section 2.8) and the eigenfrequencies of normal modes (Section 2.9), quantities that correspond to travel times.

In this chapter, we follow the approach discussed in Section 1.1.2 of treating the earth with a series of progressively more complex and, hopefully, more accurate models. We begin with the homogeneous, isotropic, elastic, layered halfspace used in Chapter 2 to derive seismic wave propagation. This approximation of uniform flat layers is often used in crust and upper mantle studies, where the distance between source and receiver is less than a few hundred kilometers. We then consider larger source–receiver distances, for which spherical geometry is required, and then the anisotropic and anelastic behavior of the earth. Throughout these discussions, we will see that although velocity varies primarily with depth, there are important lateral variations, or heterogeneities. Finally, we consider the implications of the observed heterogeneous, anisotropic, and anelastic velocity structure for the composition of the earth. Later, in Chapter 7, we discuss further how seismic data can be used to study laterally variable velocity structure.

3.2 Refraction seismology

3.2.1 *Flat layer method*

The simplest approach to the inverse problem of determining velocity at depth from travel times treats the earth as flat layers of uniform-velocity material. We thus begin by deriving the travel time curves for such a model, which show when seismic waves arrive at a particular distance from a seismic source. The travel times, especially those of waves that are critically refracted at the interfaces, are used to find the velocities of the layers and underlying halfspace and the layer thicknesses. As a result, this technique is called *refraction seismology*.

Refraction seismology is used on vastly differing scales. Near-surface structure at depths less than 100 meters can be studied using a sledge hammer or a shotgun as a source and a single receiver. Similar methods are used to study the crust and the upper mantle, with earthquake or explosion sources and many receivers at distances of hundreds of kilometers.

The simplest situation, shown in Fig. 3.2-1, is a layer of thickness h_0, with velocity v_0, overlying a halfspace with a higher velocity, v_1. We write the velocities as "v" to indicate that the analysis applies for either P or S waves. There are three basic ray paths from a source on the surface at the origin to a surface receiver at x. The travel times for these paths can be found using Snell's law.

The first ray path corresponds to a *direct wave* that travels through the layer with travel time

$$T_D(x) = x/v_0. \tag{1}$$

This travel time curve (Fig. 3.2-2) is a linear function of distance, with slope $1/v_0$, that goes through the origin.

The second ray path is for a wave reflected from the interface. Because the angles of incidence and reflection are equal,

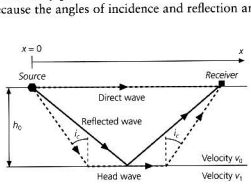

Fig. 3.2-1 Three basic ray paths for a layer over a halfspace model. The direct and reflected rays travel within the layer, whereas the head wave path also includes a segment just below the interface. For the head wave to exist, the layer velocity v_0 must be less than the halfspace velocity v_1.

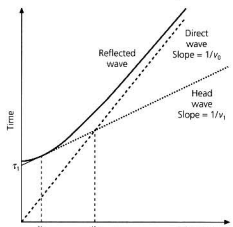

Fig. 3.2-2 Travel time versus source-to-receiver distance plot for the three ray paths in Fig. 3.2-1. The direct wave is the first arrival for receivers closer than the crossover distance x_d. Beyond x_d the head wave arrives first. The head wave exists only beyond the critical distance x_c.

the wave reflects halfway between the source and the receiver. The travel time curve can be found by noting that $x/2$ and h_0 form two sides of a right triangle, so

$$T_R(x) = 2(x^2/4 + h_0^2)^{1/2}/v_0. \tag{2}$$

This curve is a hyperbola, because it can be written

$$T_R^2(x) = x^2/v_0^2 + 4h_0^2/v_0^2. \tag{3}$$

For $x = 0$ the reflected wave goes straight up and down, with a travel time of $T_R(0) = 2h_0/v_0$. At distances much greater than the layer thickness ($x \gg h$), the travel time for the reflected wave asymptotically approaches that of the direct wave.

The third type of wave is the *head wave*, often referred to as a refracted wave. This wave results when a downgoing wave impinges on the interface at an angle at or beyond the critical angle. Its travel time can be computed by assuming that the wave travels down to the interface such that it impinges at the critical angle, then travels just below the interface with the velocity of the lower medium, and finally leaves the interface at the critical angle and travels upward to the surface. Thus the travel time is the horizontal distance traveled in the halfspace divided by v_1 plus that along the upgoing and downgoing legs divided by v_0:

$$\begin{aligned} T_H(x) &= \frac{x - 2h_0 \tan i_c}{v_1} + \frac{2h_0}{v_0 \cos i_c} \\ &= \frac{x}{v_1} + 2h_0\left(\frac{1}{v_0 \cos i_c} - \frac{\tan i_c}{v_1}\right). \end{aligned} \tag{4}$$

The last step used the fact that the critical angle (Section 2.5.5) satisfies

$$\sin i_c = v_0/v_1. \tag{5}$$

To simplify Eqn 4, we use trigonometric identities showing that

$$\cos i_c = (1 - \sin^2 i_c)^{1/2} = (1 - v_0^2/v_1^2)^{1/2} \tag{6}$$

and

$$\tan i_c = \frac{\sin i_c}{\cos i_c} = \frac{v_0/v_1}{(1 - v_0^2/v_1^2)^{1/2}}, \tag{7}$$

so Eqn 4 can be written

$$T_H(x) = x/v_1 + 2h_0(1/v_0^2 - 1/v_1^2)^{1/2} = x/v_1 + \tau_1. \tag{8}$$

Thus the head wave's travel time curve is a line with a slope of $1/v_1$ and a time axis intercept of

$$\tau_1 = 2h_0(1/v_0^2 - 1/v_1^2)^{1/2}. \tag{9}$$

This intercept is found by projecting the travel time curve back to $x = 0$, although the head wave appears only beyond the *critical distance*, $x_c = 2h_0 \tan i_c$, where critical incidence first occurs.

Because $1/v_0 > 1/v_1$, the direct wave's travel time curve has a higher slope but starts at the origin, whereas the head wave has a lower slope but a nonzero intercept. At the critical distance the direct wave arrives before the head wave. At some point, however, the travel time curves cross, and beyond this point the head wave is the first arrival even though it traveled a longer path. The *crossover distance* where this occurs, x_d, is found by setting $T_D(x) = T_H(x)$, which yields

$$x_d = 2h_0\left(\frac{v_1 + v_0}{v_1 - v_0}\right)^{1/2}. \tag{10}$$

Hence the crossover distance depends on the velocities of the layer and the halfspace and the thickness of the layer.[1]

Thus we can solve the inverse problem of finding the velocity structure at depth from the variation of the travel times observed at the surface as a function of source–receiver distance. This simple structure is described by three parameters. The two velocities, v_0 and v_1, are found from the slope of the two travel time curves. We then identify the crossover distance and use Eqn 10 to find the third parameter, the layer thickness, h_0. Alternatively, the layer thickness can be found from the reflection time or the head wave intercept (Eqn 9) at zero distance. Each of these methods exploits the fact that there is more than one ray path between the source and the receiver.

[1] A simple analogy is driving to a distant point by a route combining streets and a highway. If the destination is far enough away, it is quicker to take a longer route including the faster highway than a direct route on slower streets. The point at which this occurs depends on the relative speeds and the additional distance required to use the highway.

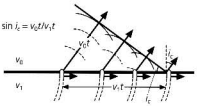

Fig. 3.2-3 Generation of an upgoing head wave by Huygens' sources due to a refracted pulse propagating along a boundary. The head wave travels in the upper layer at a slower velocity (v_0) than the refracted wave creating it, which travels in the layer below at velocity v_1. (After Griffiths and King, 1981.)

Despite this solution's elegance, the basic assumption about the travel time of the head wave may seem unsatisfying, because it is unclear why energy should follow this path. However, the result conforms with observations — the experiment diagrammed in Fig. 3.2-1 yields an arrival whose travel time is given by Eqn 8. To understand why, we can view the head wave in several ways. As shown in this chapter's problems, it corresponds to a minimum time path between the source and the receiver, so, by Fermat's principle (Section 2.5.9), we expect such a wave. Another approach, using Huygens' principle (Section 2.5.10), is to consider the refracted wave traveling horizontally below the boundary at the velocity of the half-space, generating spherical waves that propagate upward in the lower-velocity layer (Fig. 3.2-3). The spherical waves interfere to produce upgoing plane waves that leave the interface at the critical angle.[2] However, our analysis of postcritical incidence (Section 2.6.4), which showed that an evanescent wave propagates along the interface, does not fully describe the head wave. A more sophisticated analysis than is appropriate here shows that the geometry in Fig. 3.2-1 gives the head wave's travel time, but not its amplitude, because geometrical optics are not applicable. Thus, although the energy propagation is more complicated than along the geometric ray path, the travel time predicted is correct.

Seismic refraction data led A. Mohorovičić[3] in 1909 to one of the most important discoveries about earth structure. Observing two *P* arrivals (Fig. 3.2-4), he identified the first as having traveled in a deep high-velocity (7.7 km/s) layer, and the second as a direct wave in a slower (5.6 km/s) shallow layer about 50 km thick. These layers, now identified around the world, are known as the *crust* and the *mantle*. The boundary between them is known as the Mohorovičić discontinuity, or Moho. We now denote the head wave as P_n and the direct wave as P_g ("g" for "granitic"). Corresponding arrivals are also observed for *S* waves. The Moho, which defines the boundary

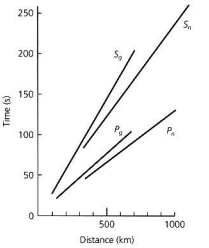

Fig. 3.2-4 Schematic of Mohorovičić's results showing the existence of a distinct crust and mantle. The travel time curves are labeled using modern nomenclature: the direct waves are P_g and S_g, and the head waves are P_n and S_n. (After Bonini and Bonini, 1979. *Eos*, 60, 699–701, copyright by the American Geophysical Union.)

between the crust and the mantle, has been observed around the world. One of the first steps in studying the nature of the crust is characterizing the depth to Moho, or crustal thickness, and the variation in P_n velocity from site to site.

Travel time plots for refraction experiments can be made by displaying seismograms in *record sections*. Because seismograms are functions of time, aligning several as a function of distance yields a travel time plot showing the different arrivals. Figure 3.2-5 shows a record section of a profile of seismograms recorded in England from explosive sources. In addition to P_n and P_g, the reflection off the Moho, known as P_mP, is well recorded. As expected, the direct and head wave travel times are linear with distance, whereas the reflection has a hyperbolic curvature. The figure is plotted as a *reduced travel time plot*, in which the time shown is the true time minus the distance divided by a constant velocity. This reduces the size of the plot, and makes waves arriving at the reducing velocity appear as a line parallel to the distance axis.

The geometry discussed here can correspond to different physical experiments. A single source can be recorded simultaneously at receivers at different distances. Alternatively, multiple sources at different distances can be recorded by a single receiver at different times. A single receiver can be moved away from a fixed source, so the same source is recorded at different distances. Similarly, a source can be moved away from a fixed receiver. Results of various experiments can be combined, using the principle of *reciprocity*, which states that the travel time is unchanged if the source and the receiver are interchanged. As a result, we can use travel time measurements without considering whether the source was at one position and the receiver at another, or the reverse. Moreover, because earth structure presumably is not changing during the experiment, data collected at different times can be combined.

[2] This situation is analogous to a bow wave from a boat or a supersonic wave from a jet airplane, in that the energy source travels faster than the wave it produces.

[3] Andrija Mohorovičić (1857–1936), working in Zagreb, Croatia (then part of the Austro-Hungarian Empire), studied travel times from earthquakes in the region using recently invented pendulum seismographs.

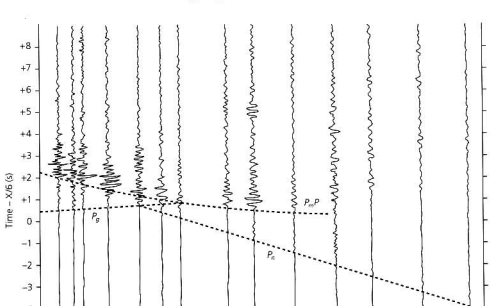

Fig. 3.2-5 Seismograms from a refraction profile, plotted with a reducing velocity of 6 km/s. The direct wave P_g, Moho head wave P_n, and Moho reflection P_mP are observed. P_g does not asymptotically approach P_mP as in Fig. 3.2-2 because the crust, instead of being homogeneous, has increasing velocity with depth. (Bott *et al.*, 1970. From *Mechanism of Igneous Intrusion*, ed. G. Newall and N. Rast, ©1970 by John Wiley & Sons Ltd. Reproduced by permission.)

Refraction data often show other arrivals in addition to P_g, P_n, and P_mP. Figure 3.2-6 shows a record section that also contains head waves P_1 and $P_2$2 from boundaries within the crust and the mantle and P_1P, a reflection off a mid-crustal interface, which is analogous to the P_mP reflection off the Moho.

Such data require a model with multiple layers. Figure 3.2-7 shows a model in which a head wave arises at each interface where the velocity increases with depth. The travel time curve for a head wave at the top of the n^{th} layer is a line with slope $1/v_n$, that can be extrapolated to its intercept on the t axis, τ_n, and written

$$T_{H_n}(x) = x/v_n + \tau_n, \tag{11}$$

where, by analogy to the layer over the halfspace case (Eqn 9),

$$\tau_n = 2\sum_{j=0}^{n-1} h_j(1/v_j^2 - 1/v_n^2)^{1/2}. \tag{12}$$

The thickness of successive layers can be found by starting with the top layer, whose thickness h_0 is given by Eqn 9 or 10, and continuing downward using the iterative formula

$$h_{n-1} = \frac{\tau_n - 2\sum_{j=0}^{n-2} h_j(1/v_j^2 - 1/v_n^2)^{1/2}}{2(1/v_{n-1}^2 - 1/v_n^2)^{1/2}}. \tag{13}$$

Thus for two layers over a halfspace, the thickness of the second layer is found by setting $n = 2$, so

$$h_1 = \frac{\tau_2 - 2h_0(1/v_0^2 - 1/v_2^2)^{1/2}}{2(1/v_1^2 - 1/v_2^2)^{1/2}}. \tag{14}$$

A few examples illustrate some other complexities of refraction experiments. If the velocity increases with depth, the travel time curve for the head wave at the top of each successive layer has a shallower slope. By contrast, a low-velocity layer (Fig. 3.2-8) does not cause a head wave, so the travel time curve does not have a first arrival with the corresponding velocity, and depths to interfaces calculated using Eqn 13 are incorrect. Another possible problem occurs if a layer is thin or has a small velocity contrast with the one below it. Although a head wave results, it may never appear as a first arrival (Fig. 3.2-9), causing a *blind zone* that can be missed in the interpretation.

3.2.2 *Dipping layer method*

The refraction method can also be applied if the interfaces between layers are not horizontal. Conducting a *reversed profile* yields the travel times for ray paths in both the down-dip and the up-dip directions. This can be done using receivers on either side of a source, sources on either side of a receiver, or both. In this geometry, the depths to the interface below the source and the receiver differ due to the dip angle, θ. Consider

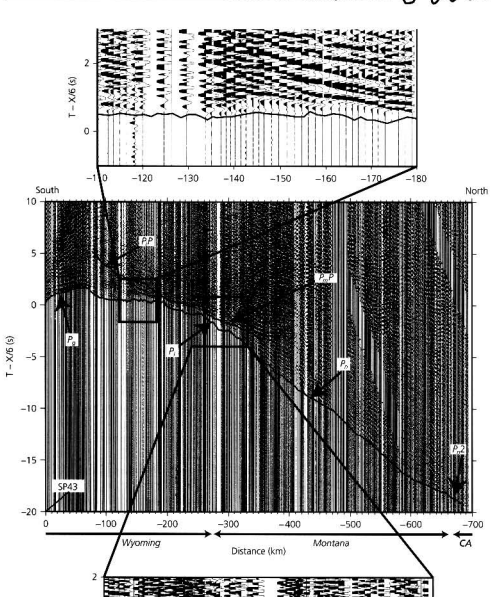

Fig. 3.2-6 Seismic refraction record section, plotted with a reducing velocity of 6 km/s. In addition to P_g, P_n, and $P_m P_n$ there are also arrivals P_c and $P_c 2$ interpreted as head waves from boundaries within the crust and the mantle, and $P_c P_c$ interpreted as a reflection off a mid-crustal interface. (Snelson *et al.*, 1998.)

the down-dip ray path (Fig. 3.2-10) from a source, below which the perpendicular distance to the interface is h_d, to a receiver at a distance x, below which the perpendicular distance to the interface is $(h_d + x \sin\theta)$. The travel time for the head wave in the down-dip direction is the sum of the distance along the interface divided by v_1 plus that for the upgoing and downgoing legs divided by v_0

$$T_d(x) = \frac{x\cos\theta - (2h_d + x\sin\theta)\tan i_c}{v_1} + \frac{(2h_d + x\sin\theta)}{v_0 \cos i_c}. \quad (15)$$

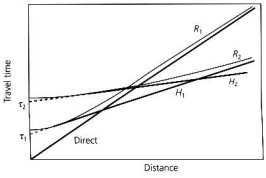

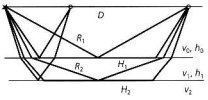

Fig. 3.2-7 Ray paths and travel times for a multilayered model in which velocity increases with depth. Each layer gives rise to a head wave H_i, whose intercept on the time axis is τ_i, and a reflection R_i. The direct wave arrival is also shown.

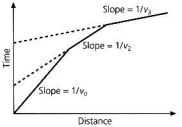

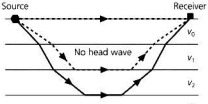

Fig. 3.2-8 Travel time curves, showing first arrivals only, for a model with three layers over a halfspace. Because the middle layer is a low-velocity layer with $v_1 < v_0$, no head wave arises at its top.

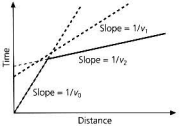

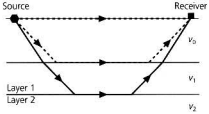

Fig. 3.2-9 Travel time curves, showing first arrivals only, for a blind zone geometry where the head wave from the top of layer 1 is never the first arrival because this layer is too thin.

Fig. 3.2-10 Head wave ray path in the down-dip direction for a dipping interface over a higher-velocity halfspace. The layer thickness is measured perpendicular to the interface.

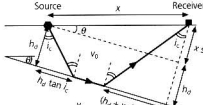

For the flat case, ($\theta = 0$), this is just Eqn 4. Simplifying using Eqns 5 and 7 yields

$$T_d(x) = \frac{x \cos\theta \sin i_c}{v_0} + \frac{(2h_d + x \sin\theta)(1 - \sin^2 i_c)}{v_0 \cos i_c}$$
$$= \frac{x \sin(i_c + \theta)}{v_0} + \frac{2h_d \cos i_c}{v_0} = \frac{x}{v_d} + \tau_d, \qquad (16)$$

which is a straight line with slope $1/v_d$ and intercept τ_d.

Similarly, the travel time for the head wave in the up-dip direction is

$$T_u(x) = \frac{x \sin(i_c - \theta)}{v_0} + \frac{2h_u \cos i_c}{v_0} = \frac{x}{v_u} + \tau_u, \qquad (17)$$

where h_u is the perpendicular distance to the interface below the receiver. Thus the apparent velocities, corresponding to the slopes of the head wave travel time curves, differ in the up-dip and down-dip directions by a factor depending on the dip angle,

$$v_u = v_0/\sin(i_c - \theta) \qquad v_d = v_0/\sin(i_c + \theta). \qquad (18)$$

The apparent velocity in the up-dip direction is greater than the halfspace velocity, and that in the down-dip direction is smaller. The time axis intercepts

$$\tau_u = 2h_u \cos i_c / v_0, \qquad \tau_d = 2h_d \cos i_c / v_0, \qquad (19)$$

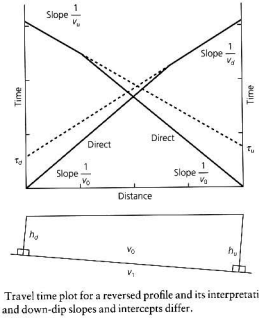

Fig. 3.2-11 Travel time plot for a reversed profile and its interpretation. The up-dip and down-dip slopes and intercepts differ.

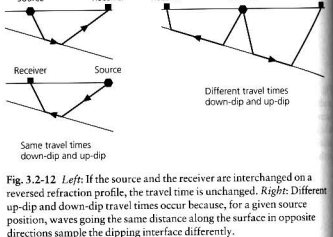

Fig. 3.2-12 *Left:* If the source and the receiver are interchanged on a reversed refraction profile, the travel time is unchanged. *Right:* Different up-dip and down-dip travel times occur because, for a given source position, waves going the same distance along the surface in opposite directions sample the dipping interface differently.

also differ. The direct wave travel time is the same in both directions, so the crossover distances differ.

The results of a reversed profile are often displayed in the form shown in Fig. 3.2-11. The time axis is common to both directions, but distance is measured from one end of the axis for the up-dip experiment and from the other for the down-dip. The slopes of the direct and head wave travel times yield the dip angle

$$\theta = \frac{1}{2}\left(\sin^{-1}\frac{v_0}{v_d} - \sin^{-1}\frac{v_0}{v_u}\right) \tag{20}$$

and the critical angle

$$i_c = \frac{1}{2}\left(\sin^{-1}\frac{v_0}{v_d} + \sin^{-1}\frac{v_0}{v_u}\right). \tag{21}$$

The halfspace velocity v_1 is found from the critical angle and v_0, and the intercept times then yield the layer thickness.

Two additional points about reversed profiles are worth noting. First, the different up-dip and down-dip head wave travel time curves do not imply that for a given pair of locations, it makes a difference whether the source is up-dip and the receiver down-dip, or the reverse (Fig. 3.2-12). By reciprocity, the two experiments give the same travel time. Thus, for a ray path connecting two points, it does not matter whether the wave travels up-dip or down-dip. By contrast, for two receivers at the same distance from a source, one up-dip and one down-dip, the travel times differ because the ray paths encounter the dipping interface at different depths. Similarly, the travel times differ for two sources at the same distance from a receiver, one up-dip and one down-dip. If the dip were zero, then the travel times would be the same for all these cases because all ray paths encounter the interface at the same depth. Another way to view this is that for a flat geometry the travel time depends only on the distance between the source and the receiver. For a dipping geometry, the position as well as the separation matters, because the depth to the interface varies.

Second, the dip found from a reversed profile is not a true dip if the profile is not perpendicular to the strike of the layer. Instead, the measured dip is an apparent dip along the profile. The true dip can be found from the apparent dips along two reversed profiles that cross at a reasonably large angle, using a standard technique in structural geology.

3.2.3 *Advanced analysis methods*

Because the analysis above has been for simple geometries and uniform-velocity layers, refraction seismology might seem of little use in understanding the real earth. Fortunately, this is not the case. The simple geometries give models that fit data reasonably well and provide starting models for more sophisticated analyses.

Data from experiments showing travel times more complex than predicted by simple geometries can be interpreted with a computer program to trace rays using Snell's law through possible velocity structures. The predicted travel time curve is found by taking rays that arrive at a given distance, and integrating the slowness along their paths (Eqn 3.1.1). Figure 3.2-13 shows a record section and the inferred velocity structure for a refraction survey in central California. Ray paths calculated through the structure shown yield a good fit to the complicated travel time data. For example, the late arrivals about 8 km from the source are interpreted as resulting from a low-velocity region associated with a set of faults. The model

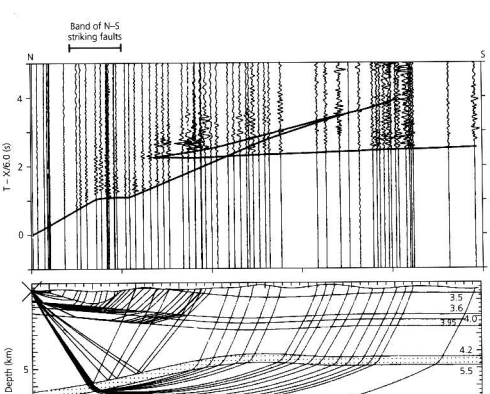

Fig. 3.2-13 Reduced travel time plot and ray tracing results for a seismic refraction survey. The solid line on the travel time plot shows the travel times predicted by the model. (Meltzer *et al.*, 1987. © Seismological Society of America. All rights reserved.)

also fits the travel times showing several velocity increases beyond this distance.

The restriction of uniform-velocity layers can also be surmounted. Geological instincts (a useful but occasionally unreliable tool) lead us to expect that rock types, and thus velocities, should often vary smoothly rather than in discrete jumps. Thus we expect velocity gradients with depth, rather than sharp interfaces. This possibility can be tested using advanced methods of analysis that predict both the travel times and the amplitudes of the expected arrivals. The amplitudes make it possible to distinguish gradients from uniform layers, even if the travel times predicted are the same. Although the methods are beyond our scope here, we discuss some results briefly.

To illustrate the relation between velocity structure and amplitudes, consider theoretical, or synthetic, seismogram record sections for the head wave, P_n, and Moho reflection, P_mP, predicted by two crustal models (Fig. 3.2-14). The seismograms were computed using a method known as reflectivity, which avoids the limitations of ray and plane wave analysis. The travel times are reduced at 8 km/s, and the direct wave is not shown. Both models have the same average velocity structure, a 30 km-thick layer of 6.5 km/s material over an 8 km/s halfspace, so the travel times are similar. However, the amplitudes of the arrivals differ noticeably because the models have different fine structure near the Moho.

For the sharp Moho model (Fig. 3.2-14, *top*) the reflected wave is small for distances less than the critical distance (*subcritical* reflection), largest near the critical distance, and large for distances greater than critical (*supercritical, postcritical*, or *wide angle* reflections). Because the boundary is sharp, this amplitude behavior is similar to that predicted for plane waves (Fig. 2.6-11). P_mP also shows the expected phase shift for reflection past critical incidence (Section 2.6.4). The head wave first appears near the critical distance, 83 km, and is small, as expected from the plane wave approximation that predicts no transmitted wave past the critical angle.

Figure 3.2-14 (*bottom*) shows the effect of velocity gradients above and below the Moho. Seismic energy trapped near the Moho yields larger P_n amplitudes than for the sharp Moho case. In addition, for subcritical distances, the reflection is smaller than without a gradient above the Moho, because it no longer reflects off a sharp interface. Hence the amplitudes

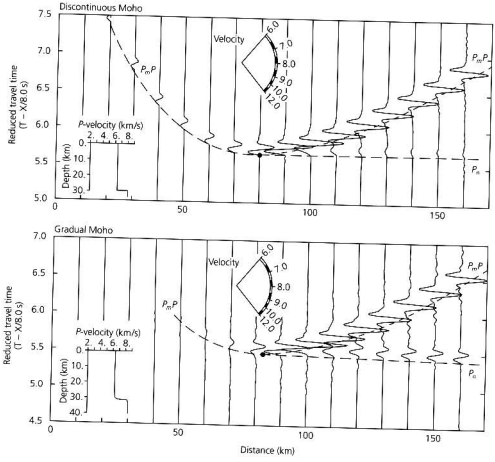

Fig. 3.2-14 Synthetic seismograms showing how the amplitudes of the head wave, P_n, and the reflected wave, P_mP, depend on the velocity structure at the Moho. Two cases with the same average-velocity structure are shown. At the *top* the Moho is a sharp transition, and at the *bottom* there are gradients above and below the Moho. The velocity scale shows the slopes of arrivals with different velocities. (After Braile and Smith, 1975.)

of P_n and P_mP indicate the presence or absence of gradients at the Moho.

Figure 3.2-15 illustrates these ideas for the oceanic crust and the mantle. Theoretical seismograms (Fig. 3.2-15, *center*) computed for a layered model that fits travel times predict strong reflections off the top of layer 3 (P_3P) and the Moho (P_mP). The observed data (Fig. 3.2-15, *bottom*) show strong P_mP reflections, suggesting a sharp Moho transition. However, strong P_1P reflections are not observed, implying that the transition between layers 2 and 3 is a gradient rather than a sharp jump. Thus, although the results of refraction studies are often reported as layered models that fit the travel times, amplitude studies are needed to show whether sharp interfaces exist.

An interesting point is that, because layers are distinguished from gradients by interpreting the amplitudes of seismic waves, this distinction depends on the wavelength of the wave used to study the structure. A reasonable approximation is that waves "see" only structures longer than their wavelengths. In other words, waves are affected by the medium properties averaged over their wavelengths. For example, the velocity structures in Fig. 3.2-16 appear identical to waves with a wavelength of 1 km, but look quite different for a wavelength of 1 m. Thus profile 3 appears as a sharp interface for waves with wavelength 1 km, a gradient for 100 m wavelength, and a stack of layers for 10 m wavelength. The velocity structure depends on the wavelengths under discussion, so a velocity "gradient" is a structure that cannot be distinguished, with the wavelengths used, from one in which velocity changes smoothly. Similarly, an "interface" is a region that cannot be distinguished from a sharp velocity change with the wavelengths used.

3.2.4 *Crustal structure*

Information about crust and upper mantle structure around the world has been acquired by refraction surveys conducted on different scales. The size of the sources and the source-to-receiver distances increase with the depth of the structures being studied. Earthquakes or large explosions, including nuclear weapons tests, have enough energy to reveal the Moho. For example, the profile in Fig. 3.2-5, which showed clear Moho arrivals, was almost 250 km long and used sources containing 136 kg of explosive. Shorter profiles are used to study structure within the crust, as in Fig. 3.2-13. The recording stations are either permanent seismic stations or, in most cases, portable seismometers. Refraction studies are also conducted

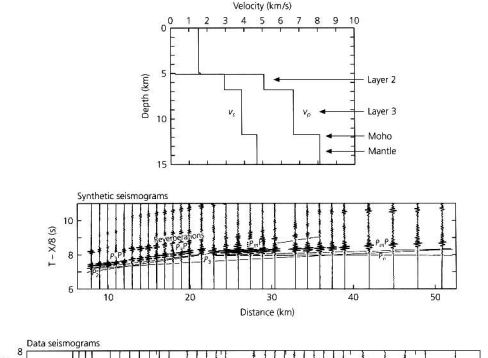

Fig. 3.2-15 *Top*: Oceanic crust model with sharp transitions between layer 1 (water), layer 2 (unconsolidated sediment), layer 3 (crustal rock), and the mantle. *Center*: Synthetic seismograms for this model. P_2, P_3 and P_m are head waves from layers 2, 3, and the mantle. P_1P and P_mP are reflections off the tops of layer 3 and the mantle. *Bottom*: Data showing an absence of the large P_2 arrivals predicted by the layered model. (After Spudich and Orcutt, 1980. *Rev. Geophys. Space Phys.*, *18*, 627–45, copyright by the American Geophysical Union.)

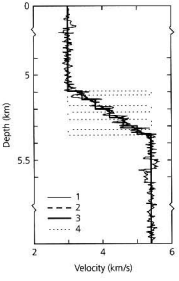

Fig. 3.2-16 Different velocity profiles that are indistinguishable when examined by using 1 km wavelength seismic waves, but distinguishable with much shorter wavelengths. (Spudich and Orcutt, 1980. *Rev. Geophys. Space Phys.*, *18*, 627–45, copyright by the American Geophysical Union.)

at sea. In some cases, disposable sonobuoys or retrievable ocean bottom seismometers are deployed, and a ship steams away firing "shots." In other cases, two ships are used. Marine refraction data (e.g., Fig. 3.2-15) are analyzed by treating the water as an upper layer of known velocity. The refraction results are combined with those from seismic reflection techniques, discussed in the next section, in which the velocity structure is derived from the travel times of subcritical reflections, rather than refractions. Refraction and reflection results are complementary and yield improved knowledge of structure.

The oceanic crust is about 7 km thick, and is relatively uniform from site to site, except at mid-ocean ridges. As a result, a single simple model like that in Fig. 3.2-15 is often applicable. By contrast, the continental crust is thicker and variable, as illustrated in Fig. 3.2-17 for a cross-section across the west coast of the United States. The thin crust beneath the Pacific Ocean thickens across the continent–ocean transition, such that beneath the coast ranges the Moho is about 25 km deep. Beneath the Sierra Nevada range, the depth to the Moho reaches 35–40 km. The refraction data also show complicated and variable-velocity structures within the crust. Thus the crust is not a uniform layer, or even a uniform set of layers, because

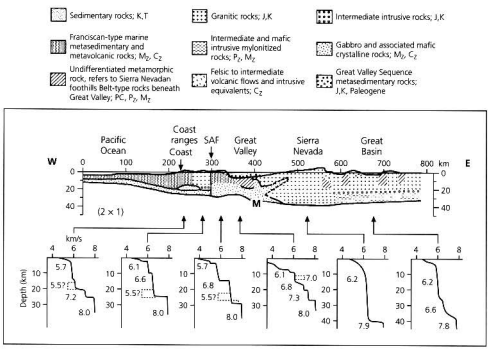

Fig. 3.2-17 Crustal velocity model and inferred geologic structure for a cross-section across the west coast of the USA. "SAF" denotes the San Andreas fault. Dashed lines indicate low-velocity zones. (After Mooney and Weaver, 1989. From *Geophysical Framework of the Continental United States*, ed. L. C. Pakiser and W. D. Mooney, with permission of the publisher, the Geological Society of America, Boulder, CO. © 1989 Geological Society of America.)

in some places it contains velocity gradients. Although early refraction studies suggested the existence of the Conrad discontinuity dividing the upper and lower crust, it now appears that high (greater than about 6.5 km/s)-velocity lower crust is present in some places but not in others. Furthermore, some areas show low-velocity zones within the crust.

Refraction studies show regional variations in crustal thickness and P_g velocities, as illustrated for North America in Fig. 3.2-18. East of ~104°W, the crust is typically thick (~42 km), and P_g velocities are high (~8.1 km/s). To the west, the crust is often thinner, with lower P_g velocities. The thin crust and low P_g velocities beneath the Basin and Range province may reflect hotter material near the surface, consistent with active extension. As seen here and globally (Fig. 3.2-19), mountain ranges often have thick crust. The thick crust is thought to be due to isostasy, whereby the excess mass of the mountains is at least partially compensated by a crustal root with density less than that of the mantle.

The continental Moho can be modeled as a simple interface for the wavelengths used in most refraction studies. However, seismic reflection studies, with shorter wavelengths, sometimes show a laminated structure of high- and low-velocity layers (Fig. 3.2-20). In other cases, however, the Moho is not observed in reflection data. Some of these complexities may reflect difficulties associated with seismic reflection studies in laterally varying media (Section 3.3). Nonetheless, the Moho appears to be a complicated transition zone 0–5 km wide, with properties varying between locations (Fig. 3.2-21). Rather than regarding the Moho as the base of a homogeneous crustal layer, it is better to view it as a zone where velocities increase rapidly with depth to values above about 7.7 km/s.

Velocity structures are often interpreted in terms of composition, as in Fig. 3.2-17. To do this, seismological results are combined with other geophysical data (e.g., gravity), geological fieldwork, and laboratory studies of the seismic velocities of rocks. The laboratory data show that velocity varies with composition, as shown in Fig. 3.2-22 for igneous rocks of the crust and upper mantle. Moreover, velocity increases with pressure and decreases with temperature. Inferences about composition are thus made by comparing predicted velocities to seismic observations. For pressures expected at greater depths, as for the lower mantle and core, laboratory experiments are more difficult, so thermodynamic calculations are also used to extrapolate experimental data to higher temperatures and pressures.

Such analyses imply that the upper continental crust has an average composition like granodiorite, whereas the upper oceanic crust is gabbroic.[4] Historically, two types of models have been suggested for the Moho. In one, the Moho divides chemically different rocks, whereas in the other, it is a phase boundary separating rocks with the same bulk chemistry but different minerals. These models correspond to different combinations of rocks on either side. Two candidates for the lower continental crust are gabbro or rocks of intermediate composition in the granulite facies. The most popular candidate for the upper mantle is peridotite, which would make the Moho a

[4] Some relevant rock and mineral nomenclature is summarized in Section 3.2.5.

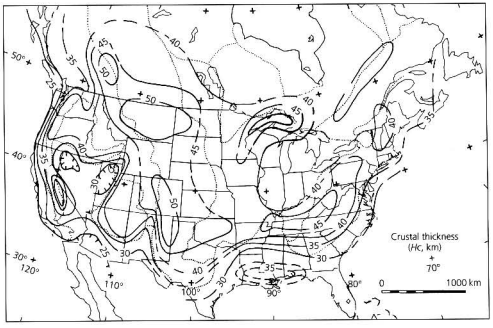

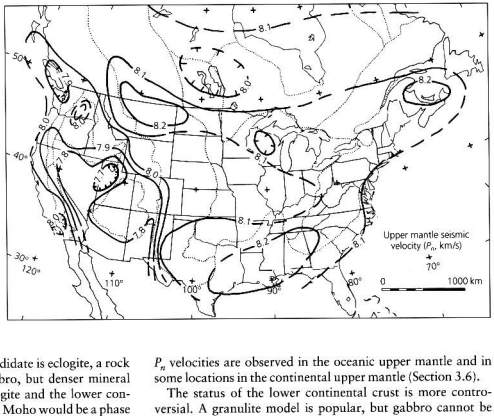

Fig. 3.2-18 Crustal thickness (depth to Moho) (*top*) and P_n velocity (*bottom*) maps for part of North America. Contour intervals are 5 km and 0.1 km/s. (Braile *et al.*, 1989. From *Geophysical Framework of the Continental United States*, ed. L. C. Pakiser and W. D. Mooney, with permission of the Geological Society of America, Boulder, CO. © 1989 Geological Society of America.)

compositional boundary. Another candidate is eclogite, a rock with the same bulk chemistry as gabbro, but denser mineral phases. If the upper mantle were eclogite and the lower continental crust gabbroic, the continental Moho would be a phase boundary. However, although eclogite and peridotite have similar seismic velocities, peridotite seems a more likely composition for the upper mantle. One of the reasons is that olivine, a major component of peridotite, yields anisotropic seismic velocities due to its crystal structure. Such anisotropic P_n velocities are observed in the oceanic upper mantle and in some locations in the continental upper mantle (Section 3.6).

The status of the lower continental crust is more controversial. A granulite model is popular, but gabbro cannot be ruled out. Similarly, the origin of the laminated structure of the Moho is still unclear. Possible explanations include metamorphosed sediments, cumulate layering, tectonic banding, and lenses of partial melt. In any event, this structure seems to be laterally variable.

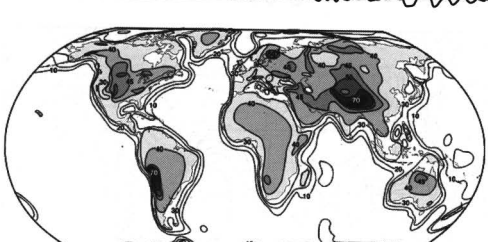

Fig. 3.2-19 Global map of crustal thickness. (Mooney *et al.*, 1998. *J. Geophys. Res.*, *103*, 727–47. Copyright by the American Geophysical Union.)

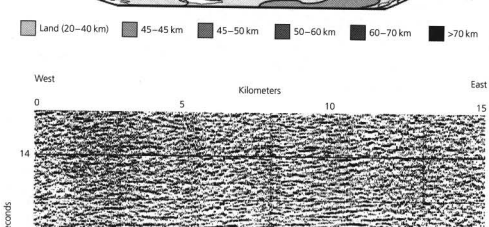

Fig. 3.2-20 Seismic reflection profile from the Wichita Mountains of southeastern Oklahoma. The "ringing" Moho reflections at 14.5–15 s in the middle of the section suggest that the Moho has a laminated velocity structure over several km. (Hale and Thompson, 1982. *J. Geophys. Res.*, *87*, 4625–35, copyright by the American Geophysical Union.)

3.2.5 Rocks and minerals

Interpreting seismological results for the crust and mantle in terms of composition requires knowing something about rocks and the minerals that compose them. Although these are complicated subjects, we summarize a few essential terms.

For our discussions of crust and upper mantle structure, the most important rocks are the igneous rocks formed by cooling a molten magma. These rocks are classified primarily by the weight percent of silica, SiO_2. A common nomenclature describes rocks as *acidic* or *silicic* for a weight percent of $SiO_2 >$ 66%, *intermediate* for 66–52%, *basic* or *mafic* for 52–45%, and *ultrabasic* or *ultramafic* for < 45%.

Physical properties of rocks, such as density and seismic velocity, depend on their mineral composition. Figure 3.2-23 summarizes the major minerals in various rocks at near-surface temperatures and pressures. Because rock names refer to a range of compositions, those shown are averages. Rocks of the same composition have different names depending on whether they form at the earth's surface (extrusive rocks) or below it (intrusive rocks). Hence an extrusive rock of gabbroic composition is a *basalt*.

Several important silicate (SiO_2-bearing) minerals are mentioned in the figure. *Quartz* is pure SiO_2. *Olivine* is a solid solution, $(Mg, Fe)_2SiO_4$, whose composition varies from pure Fe_2SiO_4 (*fayalite*) to pure Mg_2SiO_4 (*forsterite*). Due to its crystal structure, olivine has anisotropic seismic velocities. *Pyroxene* is a solid solution with end members $MgSiO_3$ (*enstatite*), $FeSiO_3$ (*ferrosilite*), $CaMg(SiO_3)_2$ (*diopside*), and $CaFe(SiO_3)_2$ (*hedenbergite*), though only certain ranges of

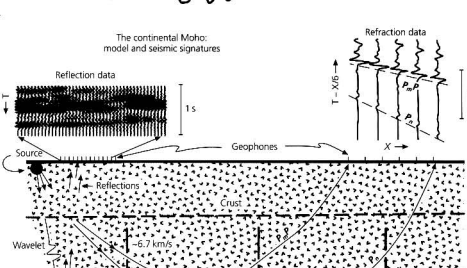

Fig. 3.2-21 Schematic model for the continental Moho as a laminated structure. Refraction studies using relatively longer wavelengths would show clear P_mP and P_m arrivals, whereas reflection studies using shorter wavelengths would show reverberations. (Braile and Chiang, 1986. *Reflection Seismology*, 257–72, copyright by the American Geophysical Union.)

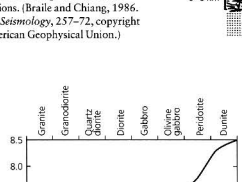

Fig. 3.2-22 Variation of P-wave velocity with lithology for crust and upper mantle rocks, at a pressure of 1.5 kbar (150 MPa). Velocity increases with decreasing silica content. (Fountain and Christensen, 1989. From *Geophysical Framework of the Continental United States*, ed. L. C. Pakiser and W. D. Mooney, with permission of the Geological Society of America, Boulder, CO. © 1989 Geological Society of America.)

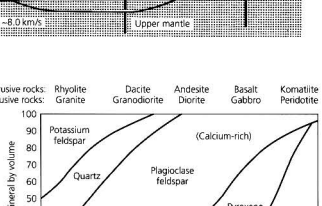

Fig. 3.2-23 Simplified igneous rock classification. Compositions are shown as the volume percent of major minerals for a rock of given silica content (horizontal axis). Thus a granodiorite of about 60% silica content contains about 20% amphibole, 5% biotite, 53% plagioclase feldspar, 17% quartz, and 5% potassium feldspar. Rock names are given for intrusive and extrusive forms.

compositions exist in nature. *Feldspar* is a solid solution with end members $CaAl_2Si_2O_8$ (*anorthite*), $NaAlSi_3O_8$ (*albite*), and $KAlSi_3O_8$ (*sanidine, orthoclase*, and *microcline*). The Na- and Ca-rich feldspars are called the *plagioclase feldspars*. A similar mineral group, the *amphiboles*, include *hornblende*, $NaCa_2(Mg,Fe)_4(Al,Fe)(Si_3AlO_{11})_2(OH)_2$. *Biotite*, $K(Mg,Fe)_3Si_3AlO_{10}(OH)_2$, and *muscovite*, $KAl_2Si_3AlO_{10}(OH)_2$, are in a group of minerals called *micas*. *Garnets* are minerals of the form $A_3B_2(SiO_4)_3$, where A is usually one of the ions Ca, Mg, or Fe, and B is typically any of Al, Fe, or Cr. Garnets are comparatively dense, and thus significant for discussions of phase changes.

The figure describes rocks in terms of their mineralogy at surface conditions. With increasing pressure due to increasing depth in the earth, minerals transform to denser phases. Thus, for example, a gabbro containing plagioclase feldspar, pyroxene, and olivine transforms to a chemically identical eclogite rock containing quartz, pyroxene, and garnet. Hence

an argument against eclogite being a major component of the upper mantle is that, by contrast with peridotite, it does not contain olivine and would not yield the observed anisotropic P_n velocities. However, the gabbro-to-eclogite transformation may occur in subducting slabs (Section 5.4.2) and play a role in causing earthquakes there.

3.3 Reflection seismology

In the last section, we concentrated on the use of refracted arrivals to infer velocity structure with depth, and noted that reflected arrivals also contain valuable information for this purpose. Studies using the reflected arrivals, known as *reflection seismology*, determine velocities within the crust, and thus are essential in oil and gas exploration. As a result, data acquisition and processing methods have often been developed first by reflection seismologists. For example, digital data were generally used in exploration before they became common in earthquake studies. Similarly, because reflection data are densely sampled in space and time, and the mathematics of wave propagation in a layered medium is simpler than for a spherical earth, techniques are often first developed with reflection data. In this section we survey basic concepts in reflection seismology, some of which we later apply to earthquakes and the spherical earth.

3.3.1 *Travel time curves for reflections*

We first consider the simplest geometry: a flat layer of uniform-velocity material underlain by a halfspace with a higher velocity (Fig. 3.2-1). Although most applications use P waves, we write the velocity as "v" because the results also apply to S waves. For a layer of thickness h_0 with velocity v_0, we saw in Section 3.2.2 that the travel time as a function of source-to-receiver distance, known as *offset* in reflection seismology, is

$$T(x)^2 = x^2/v_0^2 + 4h_0^2/v_0^2 = x^2/v_0^2 + t_0^2. \tag{1}$$

The travel time curve $T(x)$ is a hyperbola (Fig. 3.3-1) that intercepts the T axis at $t_0 = 2h_0/v_0$, the travel time at zero offset. This time is called the two-way vertical travel time, because the corresponding ray traveled vertically down to the reflector and back. Although this curve is the same as the "reflected wave" curve in Fig. 3.2-2, the convention in reflection seismology is to plot time increasing downward,[1] because later arrivals reflect deeper in the earth.

The layer velocity is found from the slope of the hyperbola. Because the slope decreases with increasing velocity, "flatter" travel time curves indicate higher velocities. To see this, note that a plot of $T(x)^2$ versus x^2 has slope $1/v_0^2$. Alternatively, the variation in travel time with offset is often stated in terms of

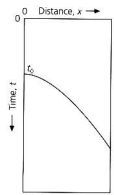

Fig. 3.3-1 The travel time curve for a reflection off a flat interface is a hyperbola, with the minimum at $x = 0$ corresponding to a vertical ray path. The slope is zero at $x = 0$ and increases with the offset distance.

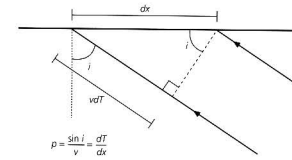

Fig. 3.3-2 Two rays showing the relationship between the angle of incidence, ray parameter, and the slope of the travel time curve for a flat medium.

normal moveout (NMO), the difference between the travel time at some offset and that at zero offset,

$$T(x) - t_0 = (x^2/v_0^2 + t_0^2)^{1/2} - t_0. \tag{2}$$

Once the velocity is found, the layer thickness is given by the vertical travel time.

To see the relation between the travel time curve and ray paths, consider the ray paths to two points dx apart, which differ in travel time by dT (Fig. 3.3-2). Because the ray paths differ in length by vdT, the angle of incidence can be found using

$$\sin i = \frac{vdT}{dx} \tag{3}$$

or, in terms of the ray parameter p (Section 2.5.7),

$$p = \frac{\sin i}{v} = \frac{dT}{dx}. \tag{4}$$

This is consistent with our earlier definition of the ray parameter as the reciprocal of the apparent velocity along the

[1] Earthquake seismologists generally follow the opposite convention.

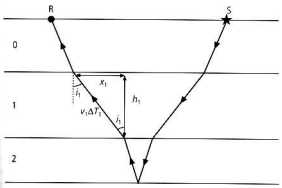

Fig. 3.3-3 Ray geometry for a reflection in a flat-layered medium. Layer thicknesses are h_j, horizontal distances traveled in the layers are x_j, and one-way travel times spent in the layers are ΔT_j.

surface of the wave front, which moves a distance dx in time dT, because

$$p = 1/c_x = 1/(dx/dT). \tag{5}$$

Thus the ray parameter and the angle of incidence of the ray emerging at a distance x can be found from dT/dx, the slope of the travel time curve evaluated at x. From Eqn 2, the slope is zero at $x = 0$ and then increases with offset; so the angle of incidence is nearly zero (vertical incidence) at short distances and becomes closer to 90° (horizontal) at larger distances (Fig. 3.3-1).

This lets us find the travel time curve for reflections in a geometry with multiple horizontal layers. Figure 3.3-3 shows that the reflection R_{n+1} from the top of the $(n+1)^{\text{th}}$ layer (or the bottom of the n^{th} layer) has traveled through n layers, each of thickness h_j and velocity v_j. Such rays, which have been reflected only once, are known as primary reflections. Because, by Snell's law, the ray parameter p is constant along a ray, the incidence angles i_j in each layer can be found from the incidence angle i_0 in the top layer,

$$p = \frac{\sin i_j}{v_j} = \frac{\sin i_0}{v_0}. \tag{6}$$

A downgoing ray, which travels a horizontal distance x_j in the j^{th} layer, spends a time ΔT_j in the layer. Thus, in going down and up again, the ray travels a total horizontal distance

$$x(p) = 2\sum_{j=0}^{n} x_j = 2\sum_{j=0}^{n} h_j \tan i_j \tag{7}$$

in a total time

$$T(p) = 2\sum_{j=0}^{n} \Delta T_j = 2\sum_{j=0}^{n} \frac{h_j}{v_j \cos i_j}. \tag{8}$$

We explicitly write $x(p)$ and $T(p)$, because the two sums are formulated in terms of the ray parameter. To see how they allow us to compute the corresponding travel time curve $T(x)$, consider a single layer, where $x_0 (= x/2)$ is the horizontal distance along each of the downgoing and upgoing legs. In this case, Eqn 8 becomes

$$T(x) = 2[(x/2)^2 + h_0^2]^{1/2}/v_0, \tag{9}$$

because

$$\cos i_0 = h_0 (x_0^2 + h_0^2)^{-1/2}. \tag{10}$$

Hence Eqn 8 yields Eqn 9, which is equivalent to the relation we derived earlier showing that the travel time curve for the reflection is a hyperbola (Eqn 1).

For multiple layers, we approximate the travel time curve for the reflection R_{n+1} off the top of the $(n+1)^{\text{th}}$ layer as a hyperbola,

$$T(x)^2_{n+1} = x^2/\bar{V}_n^2 + t_n^2, \tag{11}$$

and find the two parameters, $\bar{V}_n$ and t_n. t_n is the total two-way (up and down) vertical travel time at zero offset, which is twice the sum of the one-way vertical travel times Δt_j for each layer

$$t_n = 2\sum_{j=0}^{n} \Delta t_j = 2\sum_{j=0}^{n} (h_j/v_j). \tag{12}$$

The velocity term, $\bar{V}_n$, is a little trickier. From the geometry, the distance traveled by the downgoing ray in layer j is

$$x_j = v_j \Delta T_j \sin i_j = (v_j^2/v_0)\Delta T_j \sin (i_0), \tag{13}$$

where the last step used Snell's law (Eqn 6). Hence, by Eqn 7, the total distance, x, can be written

$$x = 2\sum_{j=0}^{n} x_j = 2\frac{\sin i_0}{v_0}\sum_{j=0}^{n} v_j^2 \Delta T_j. \tag{14}$$

Because the ray parameter is constant along a ray, the slope of the travel time curve is, by Eqn 4,

$$\frac{dT}{dx} = \frac{\sin i_0}{v_0} = x/(2\sum_{j=0}^{n} v_j^2 \Delta T_j). \tag{15}$$

For the hyperbolic approximation (Eqn 11), the slope of the travel time curve is

$$\frac{dT}{dx} = \frac{x}{\bar{V}_n^2 T}, \tag{16}$$

so we define

$$\bar{V}_n^2 = (2\sum_{j=0}^{n} v_j^2 \Delta T_j)/T. \tag{17}$$

Because this was derived for an arbitrary incidence angle, vertical incidence can be used for simplifications, so in each layer the travel time equals the one-way vertical travel time, $\Delta T_j = \Delta t_j$, and the total travel time is $T = 2\sum_{j=0}^{n} \Delta t_j$. Hence

$$\bar{V}_n^2 = \left(\sum_{j=0}^{n} v_j^2 \Delta t_j\right) \Big/ \left(\sum_{j=0}^{n} \Delta t_j\right). \tag{18}$$

$\bar{V}_n$, the appropriate average velocity for the travel time curve, is the time-weighted *root mean square*, or *rms*, velocity for the first n layers. This hyperbolic approximation and the exact solutions agree well except for large offsets.

These results let us find the layer velocities from the travel time curves. Given a reflection from the top of the n^{th} layer, with vertical two-way travel time t_{n-1} and rms velocity $\bar{V}_{n-1}$, and a reflection from the top of the $(n+1)^{\text{th}}$ layer, with vertical two-way travel time t_n and rms velocity $\bar{V}_n$, the velocity in the n^{th} layer is

$$v_n^2 = \frac{\bar{V}_n^2 t_n - \bar{V}_{n-1}^2 t_{n-1}}{t_n - t_{n-1}}. \tag{19}$$

This relationship is called the *Dix equation*.[2] The resulting velocity, called an *interval velocity*, is better determined for larger offsets, where the slope of the travel time curve is greater. Because the later reflections have higher velocities, and hence flatter travel time curves (Fig. 3.3-4), larger offsets are required to determine velocities at greater depths.

Travel time calculations are more complicated for dipping layers. Figure 3.3-5 shows the geometry for a reflector of dip θ, whose depth along the perpendicular to the reflector below the origin is h. The travel times can by derived using an imaginary source on the line from the surface source normal to the reflector, at the same distance below the layer, so that travel times from the imaginary source to the receivers are the same as from the true source. Applying the law of cosines to triangle RIS shows that

$$\begin{aligned} T^2 &= [x^2 + 4h^2 - 4hx\cos(\theta + \pi/2)]/v_0^2 \\ &= [x^2 + 4h^2 + 4hx\sin\theta]/v_0^2. \end{aligned} \tag{20}$$

This travel time curve is a hyperbola with minimum at $-2h\sin\theta$, so it is not symmetric about $x = 0$. Reflections from a stack of dipping layers yield travel time curves of approximately this form.

It is sometimes useful to think of the earth as having a continuous distribution of velocity with depth, $v(z)$, rather than a stack of discrete layers, each with uniform velocity. The expressions for the ray path and travel time of a ray with ray parameter p for discrete layers can be generalized. The ray path (Fig. 3.3-6) is given by Snell's law, because the ray parameter,

[2] Named after its discoverer, pioneering exploration seismologist C. Hewitt Dix (1905–84).

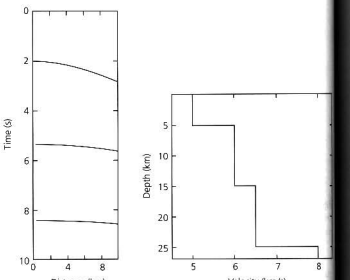

Fig. 3.3-4 Travel time curves for reflections (*left*) from a layered structure (*right*) corresponding to continental crust. Reflections from deeper interfaces are flatter, or have shallower slopes, due to the increase of velocity with depth.

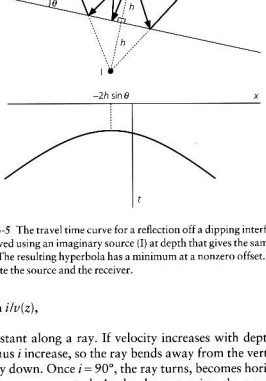

Fig. 3.3-5 The travel time curve for a reflection off a dipping interface can be derived using an imaginary source (I) at depth that gives the same travel times. The resulting hyperbola has a minimum at a nonzero offset. S and R denote the source and the receiver.

$$p = \sin i/v(z), \tag{21}$$

is constant along a ray. If velocity increases with depth, sin i and thus i increase, so the ray bends away from the vertical on its way down. Once $i = 90°$, the ray turns, becomes horizontal, and then goes upward. At the deepest point, the turning, or bottoming, depth z_p, the velocity is the reciprocal of the ray parameter, $p = 1/v(z_p)$. If on some portion of the ray path the velocity decreases with depth, the ray bends toward the

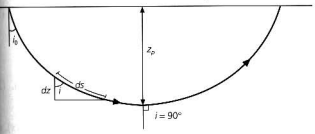

Fig. 3.3-6 Ray path in a medium with velocity increasing smoothly with depth. The ray parameter is constant along the ray path, so the angle of incidence changes as the velocity changes. The incidence angle is smallest at the surface, where velocity is lowest, and is 90° at the bottoming depth, z_p.

vertical. The ray does not turn upward until it gets below the low-velocity region.

We thus replace the sums over layer thickness h_j with integrals over depth, such that the expression for the distance traveled by the ray (Eqn 7) becomes

$$x(p) = 2\int_0^{z_p} \tan i \, dz = 2p\int_0^{z_p} \left(\frac{1}{v^2(z)} - p^2\right)^{-1/2} dz, \tag{22}$$

because

$$\sin i = pv(z) \quad \text{and} \quad \cos i = (1 - \sin^2 i)^{1/2} = (1 - p^2v^2(z))^{1/2}. \tag{23}$$

This is sometimes written in terms of the slowness, the reciprocal of velocity, as

$$u(z) = 1/v(z), \tag{24}$$

so that

$$x(p) = 2p\int_0^{z_p} \frac{dz}{(u^2(z) - p^2)^{1/2}}. \tag{25}$$

Similarly, the travel time sum (Eqn 8) becomes

$$T(p) = 2\int_0^{z_p} \frac{dz}{v(z)\cos i} = 2\int_0^{z_p} \frac{dz}{v(z)(1 - p^2v^2(z))^{1/2}}$$

$$= 2\int_0^{z_p} \frac{u^2(z)dz}{(u^2(z) - p^2)^{1/2}}. \tag{26}$$

This integral is valid everywhere except at the exact bottom of the curve, where $u(z)$ equals p. A useful way to view this is to note that the ray path (Fig. 3.3-6) can be written as an integral over ds, where $dz = \cos i \, ds$. The travel time is thus

$$T(p) = \int \frac{ds}{v(z)} = \int u(z)ds, \tag{27}$$

the integral of the slowness along the ray path. Slowness, though less intuitive to use than velocity,[3] can lead to simpler formulations.

3.3.2 *Intercept-slowness formulation for travel times*

So far, we have given travel time curves as $T(x)$, the travel time as a function of distance. We now develop an alternative formulation that offers interesting insights and is useful for data analysis. To do so, we note that ΔT_j, the one-way travel time in the j^{th} layer with velocity v_j, is related to the thickness, h_j, and the horizontal distance traveled, x_j (Fig. 3.3-3), by

$$v_j\Delta T_j = (x_j^2 + h_j^2)^{1/2}. \tag{28}$$

The incidence angle i_j for this ray satisfies

$$\sin i_j = \frac{x_j}{(x_j^2 + h_j^2)^{1/2}} = \frac{x_j}{v_j\Delta T_j} \quad \cos i_j = \frac{h_j}{(x_j^2 + h_j^2)^{1/2}} = \frac{h_j}{v_j\Delta T_j}. \tag{29}$$

We rewrite Eqn 28 as

$$v_j\Delta T_j = \frac{x_j^2 + h_j^2}{(x_j^2 + h_j^2)^{1/2}} = x_j \sin i_j + h_j \cos i_j, \tag{30}$$

or

$$\Delta T_j = \frac{x_j \sin i_j}{v_j} + \frac{h_j \cos i_j}{v_j} = p_j x_j + \eta_j h_j, \tag{31}$$

where

$$p_j = (\sin i_j)/v_j = \sin i_j u_j \quad \text{and} \quad \eta_j = (\cos i_j)/v_j = \cos i_j u_j. \tag{32}$$

Thus in layer j we have entities introduced in Section 2.5.7: p_j is the ray parameter, or horizontal slowness, and η_j is the vertical slowness. These are the components of the slowness vector that has magnitude equal to the slowness, and points in the direction of wave propagation. Hence u_j, the slowness in the layer, is

$$u_j^2 = 1/v_j^2 = p_j^2 + \eta_j^2. \tag{33}$$

By Eqn 31, the travel time a ray spends in a layer is the sum of the horizontal slowness times the horizontal distance traveled and the vertical slowness times the vertical thickness. The total travel time is the sum over all layers, with a factor of two to account for both downgoing and upgoing legs,

[3] It is somehow harder to think of a zone of high slowness than a low-velocity zone.

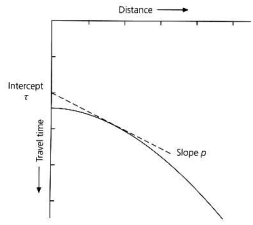

Fig. 3.3-7 Relation between the travel time curve $T(x)$ and the line tangential to a point on it, which has a slope, or slowness, p and a time axis intercept τ.

$$T(x) = 2\sum_{j=0}^{n} \Delta T_j = 2\sum_{j=0}^{n} p_j x_j + 2\sum_{j=0}^{n} \eta_j h_j. \tag{34}$$

By Snell's law, the horizontal ray parameter is constant along the ray path, so $p_j = p$, and

$$T(x) = px + 2\sum_{j=0}^{n} \eta_j h_j, \tag{35}$$

where $x = 2\sum_{j=0}^{n} x_j$ is the total horizontal distance traveled. This formulation is equivalent to the way we formulated the travel time as the scalar product of the distance and slowness vectors (Eqn 2.5.34).

Formulating the travel time curve in this way gives interesting insight. We define

$$T(x) = px + \tau(p), \tag{36}$$

where the function

$$\tau(p) = 2\sum_{j=0}^{n} \eta_j h_j = 2\sum_{j=0}^{n} (1/v_j^2 - p^2)^{1/2} h_j = 2\sum_{j=0}^{n} (u_j^2 - p^2)^{1/2} h_j. \tag{37}$$

Because p is the slope of the travel time curve (dT/dx) and hence of a line tangential to it at the point (T, x), τ is the intercept of the tangent line with the time axis (Fig. 3.3-7). In general τ and p differ for different points on the travel time curve, so the travel time curve can be described by the values of either (T, x) or (τ, p). Thus the function $\tau(p)$ is called the *intercept-slowness* representation of the travel time curve. Although less intuitive, the $\tau(p)$ formulation is equivalent to $T(x)$.

Given that the slope of the travel time curve $T(x)$ has special significance, it is natural to investigate the slope of the function $\tau(p)$. To do this, we write Eqn 36 with the ray parameter, rather than the distance, as the independent variable,

$$\tau(p) = T(p) - px(p), \tag{38}$$

and differentiate

$$\frac{d\tau}{dp} = \frac{dT}{dp} - p\frac{dx}{dp} - x(p) = \frac{dT}{dx}\frac{dx}{dp} - p\frac{dx}{dp} - x(p) = -x(p). \tag{39}$$

Thus, just as p is the slope of the travel time curve, $T(x)$, the distance, x, is minus the slope of the $\tau(p)$ curve.

To illustrate these ideas, we show that the $\tau(p)$ formulation gives the travel time curve for the reflected wave in a layer over a halfspace. Figure 3.3-3 shows that $x_0 = x/2$, so, using Eqn 32,

$$p = \frac{(x/2)}{v_0[(x/2)^2 + h_0^2]^{1/2}}, \quad \eta_0 = \frac{h_0}{v_0[(x/2)^2 + h_0^2]^{1/2}}. \tag{40}$$

Hence, by Eqns 36 and 37, the travel time curve is

$$\begin{aligned} T(x) &= px + 2\eta_0 h_0 = \frac{(x^2/2) + 2h_0^2}{v_0[(x/2)^2 + h_0^2]^{1/2}} \\ &= 2[(x/2)^2 + h_0^2]^{1/2}/v_0, \end{aligned} \tag{41}$$

which is the familiar hyperbola (Eqn 9).

To see how this travel time curve appears when written as $\tau(p)$, we write Eqn 37 for a layer over a halfspace:

$$\tau(p) = 2(1/v_0^2 - p^2)^{1/2} h_0. \tag{42}$$

This can also be written as

$$(v_0^2\tau^2)/(4h_0^2) + v_0^2 p^2 = 1, \tag{43}$$

which is an ellipse whose axes are the τ and p axes (Fig. 3.3-8). It intersects the τ axis at ($\tau = t_0 = 2h_0/v_0$, $p = 0$), and the p axis at ($\tau = 0$, $p = 1/v_0$). Both these points have significance. The first, where the travel time curve has zero slope and the time axis intercept is the vertical two-way travel time, corresponds to the zero-offset point $x = 0$.

The second, where the travel time curve has slope $1/v_0$ and time axis intercept 0, is the $\tau(p)$ position of the linear travel time curve for the direct wave. Hence the line for the direct wave maps to a point in the $\tau(p)$ plane that is on the ellipse describing the reflected wave. To understand why this occurs, we use the fact that distance is minus the derivative of the $\tau(p)$ curve (Eqn 39) and differentiate Eqn 42, giving

$$x(p) = -d\tau/dp = 2ph_0(1/v_0^2 - p^2)^{-1/2}, \tag{44}$$

so at the point $p = 1/v_0$, $x = \infty$. This makes sense, because as $x \to \infty$, the reflected wave is asymptotic to the direct wave (Fig. 3.2-2).

The head wave is easily mapped into the $\tau(p)$ plane, because its travel time curve (Eqn 3.2.8) is

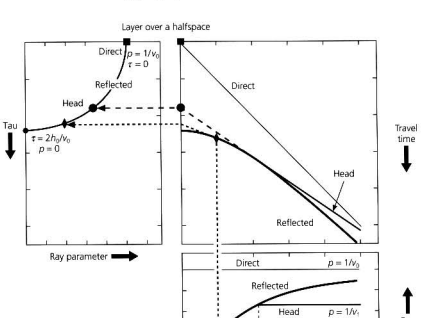

Fig. 3.3-8 Travel time curves $T(x)$ for a layer over a halfspace and their representation in the (τ, p) plane. Each point on the $T(x)$ curves has a slope (ray parameter) p and intercept τ. The linear travel time curves for the direct and head waves each map into a point (square and circle) in the (τ, p) plane. The hyperbolic travel time curve for the reflection maps into an ellipse in the (τ, p) plane. Note how an arbitrary point on the reflection's travel time curve, marked by the diamond, maps into the other two curves.

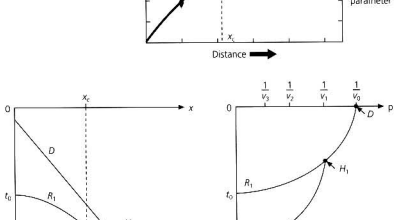

Fig. 3.3-9 Relation between the travel time curve $T(x)$ and the function $\tau(p)$ for multiple layers over a halfspace. D denotes the direct wave; R_i and H_i are reflections and head waves at the top of the i^{th} layer; x_c is the critical distance for H_1. (After Diebold and Stoffa, 1981. Reproduced by permission of the Society of Exploration Geophysicists.)

$$T_H(x) = x/v_1 + 2h_0(1/v_0^2 - 1/v_1^2)^{1/2}$$
$$= x/v_1 + \tau_1, \qquad (45)$$

a line with slope equal to the reciprocal of the halfspace velocity, $p = 1/v_1$, and intercept τ_1. Thus the head wave maps into a point on the ellipse describing the reflected wave, corresponding to the critical distance x_c where the head and reflected waves are the same. To see this, note that for $p = 1/v_1$, Eqn 44 gives

$$x(p) = -d\tau/dp = 2h_0 v_0 (v_1^2 - v_0^2)^{-1/2} = x_c. \qquad (46)$$

This point divides the ellipse describing the reflected wave into a subcritical portion, between the τ axis and the head wave, and a postcritical portion, between the head wave and the p axis. We will see shortly that the fact that different arrivals have distinct locations in the $\tau(p)$ plane provides the basis for techniques that can separate these arrivals.

This analysis can be extended to more complex geometries. For multiple layers, the $\tau(p)$ curves corresponding to reflections off successive layers are all portions of different ellipses (Fig. 3.3-9). For a continuous velocity distribution, the summation for τ (Eqn 37) becomes an integral

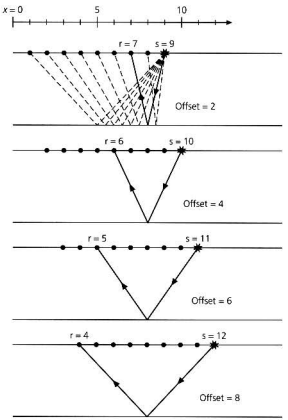

Fig. 3.3-10 Schematic geometry of a multichannel seismic reflection survey with a single source (star) and eight receivers (dots) moving along a survey line. Each physical experiment produces eight seismograms corresponding to ray paths (dashed lines) with a single source location and a range of receiver locations. Four seismograms from different source and receiver positions, corresponding to the ray paths shown by solid lines, sample the same point at depth on a flat reflector. These have the same midpoint halfway between source and receiver, but different source-to-receiver offsets.

$$\tau(p) = 2\int_0^{z_p} \eta(z)dz = 2\int_0^{z_p} (1/v^2(z) - p^2)^{1/2}dz = 2\int_0^{z_p} (u^2(z) - p^2)^{1/2}dz. \tag{47}$$

Formulating travel time curves as $\tau(p)$ is useful for some techniques that invert for velocity structure.

3.3.3 *Multichannel data geometry*

A feature of reflection seismology is *multichannel* geometry, the use of multiple source and receiver locations, so that points on reflecting interfaces are sampled repeatedly. Figure 3.3-10 illustrates how such coverage is accomplished by combining experiments performed with a seismic source and an array of eight receivers at fixed distances from the source. Each time the source is activated, eight seismograms, or *traces*, are recorded.

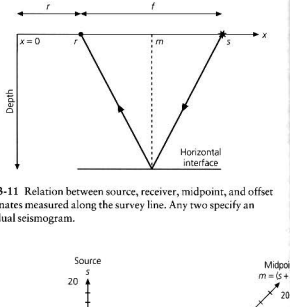

Fig. 3.3-11 Relation between source, receiver, midpoint, and offset coordinates measured along the survey line. Any two specify an individual seismogram.

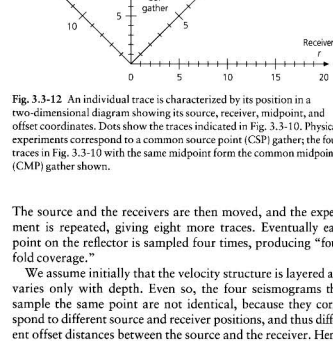

Fig. 3.3-12 An individual trace is characterized by its position in a two-dimensional diagram showing its source, receiver, midpoint, and offset coordinates. Dots show the traces indicated in Fig. 3.3-10. Physical experiments correspond to a common source point (CSP) gather; the four traces in Fig. 3.3-10 with the same midpoint form the common midpoint (CMP) gather shown.

The source and the receivers are then moved, and the experiment is repeated, giving eight more traces. Eventually each point on the reflector is sampled four times, producing "four-fold coverage."

We assume initially that the velocity structure is layered and varies only with depth. Even so, the four seismograms that sample the same point are not identical, because they correspond to different source and receiver positions, and thus different offset distances between the source and the receiver. Hence each trace is a record of displacement, or pressure, as a function of time, t, $u(s, r, t)$, characterized by the source and receiver positions.

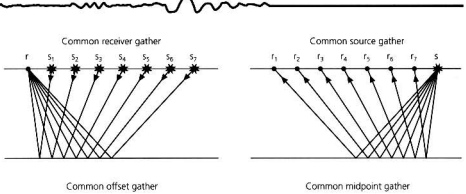

Fig. 3.3-13 Schematic of the four different gather types.

The data are analyzed by grouping the seismograms that sampled the same point on the reflector. In this flat-layered geometry, these seismograms have the same point, known as the *midpoint*, halfway between the source and the receiver. For each midpoint, there is a set of traces with different offsets. The midpoint m and offset f are defined in terms of the source location s and the receiver position r as

$$m=(s+r)/2, \quad f=(s-r). \tag{48}$$

Thus an individual seismogram is specified by either the source and receiver positions, or the midpoint and offset (Fig. 3.3-11). These are plotted using two perpendicular axes (Fig. 3.3-12), one for the source location and one for the receiver position. The midpoint and offset for each seismogram are indicated by distance along axes 45° from the s and r axes. Note that the scales on these axes differ from the other two.

To illustrate this relationship, consider the four experiments in Fig. 3.3-10, with eight receivers and a single source. Each experiment produced data at points, shown by dots, with constant source position and successive receiver positions. Successive experiments yielded data along a similar horizontal line, but displaced by the motion of the source and the receiver.

The data can be sorted and combined in various ways that need not correspond to an actual experiment (Fig. 3.3-13). Each experiment corresponds to a set of records with the same source position, a *common source point*, or *CSP*, gather. Traces with the same midpoint and different offsets can be grouped in a *common midpoint*, or *CMP*, gather. Similarly, common receiver point and common offset gathers can be formed.

Ordering traces by midpoint and offset makes no distinction between a source at position a and a receiver at position b, or the reverse. This assumption is justified by the principle of reciprocity, by which these two geometrices should produce identical seismograms. Thus a common receiver point gather can simulate a reversed profile (Section 3.2.2) because, by reciprocity, it gives the same data as a common source point gather shot in the opposite direction.

Later in this section, we will discuss a few aspects of the data collection process. The sources can be explosives, sound sources in water, or vibration sources on land. The source coordinate is thus sometimes referred to as a source point, shot point, or vibration point. The receivers are typically single-component vertical seismometers, known as geophones, for land applications, and pressure transducers, or hydrophones, for marine surveys. The receiver coordinate is thus often termed the geophone coordinate. Generally large numbers of receivers, which are themselves groups of receivers, are used. Increasingly, data are collected over two-dimensional areas, and so are processed to yield three-dimensional velocity structures.

3.3.4 *Common midpoint stacking*

Because the traces in a CMP gather have ideally sampled the same subsurface point with different offsets, they can be combined to enhance reflected arrivals. The process begins with a set of traces showing the data as a function of offset and time. The data contain "signals" of interest, primary reflections from interfaces that are used to determine velocity structure with depth. The data also contain "noise," arrivals of no interest, including direct waves, head waves,[4] surface waves (sometimes termed "ground roll"), and waves from the source that travel in the air. The data may also contain arrivals (Fig. 3.3-14) that have been reflected more than once, which are known as *multiples*, by contrast with the once-reflected primary reflections.

To enhance primary reflections and suppress everything else, we exploit the fact that the arrival times of various signals

[4] In the previous section we focused on direct and head waves, illustrating the adage that "one person's signal is another's noise."